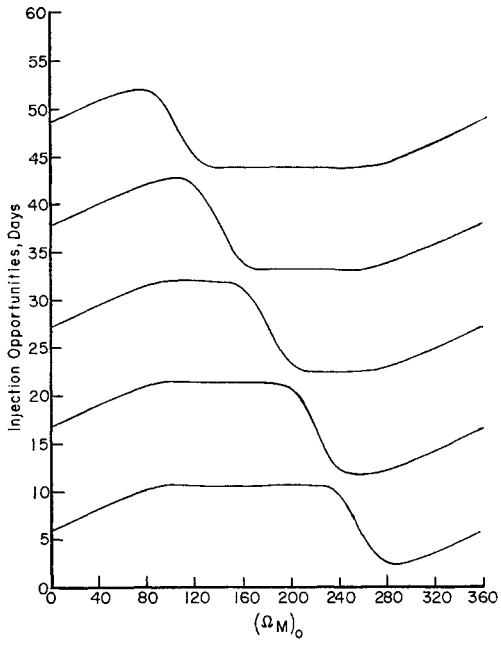

Fig 2 In-plane injection opportunities for all nominal lunar positions

nominal values of Ω_M These curves show that for the majority of the nominal injection conditions the opportunities for injection, after the first opportunity, occur about every 10 5 days The variations in ϕ at the injection opportunities for this case is between 1 5° and 58 5°

References

[1] Blitzer, L , "Apsidal motion of an IGY satellite orbit," J Appl Phys **28**, 1362 (1957)

[2] Wells, W R , "The influence of precession of earth rendezvous orbits on lunar mission requirements," NASA TN D-1512 (1962)

A Calorimeter Study of a Magnetically Stabilized Arc-Heater

ROGER B STEWART*
NASA Langley Research Center, Hampton, Va

Nomenclature

A = area, ft²
C_d = nozzle discharge coefficient, $\dot{m}_{\text{actual}}/\dot{m}_{\text{ideal}}$
d = throat diameter, in
h = enthalpy, Btu/lb
$\dot{m}$ = mass flow rate, lb/sec
p = pressure, psi
T = temperature, °R
u = velocity, fps
γ = ratio of specific heats, C_p/C_v
ρ = density, lb/ft³

Superscript

* = sonic throat conditions

Subscripts

cold = arc off running conditions
hot = arc on running conditions
t = total conditions

Received November 15, 1963
* Aerospace Engineer Member AIAA

Introduction

TEMPERATURES in the stagnation chambers of arc-heated wind tunnels are often obtained by means of a sonic throat analysis using measured values of stagnation pressure, mass flow, and throat area A recent study of the total energy of air exhausting from a magnetically stabilized arc-heater indicates that, if the effective throat area is taken as being equal to the geometric throat area in the sonic flow analysis, large errors in stagnation enthalpy determination can result Within a properly selected range of operating conditions, a particular form of the sonic flow relations can be used to give good agreement with the calorimeter results

Experimental Apparatus

The facility used for this investigation was a modified version of the arc-heater described in Ref 1 The heater employed a 12,000 gauss magnetic field to rotate the arc between a center cathode and the cylindrical walls of the arc chamber (anode) The heater had a 4-in long arc chamber and a $2\frac{1}{2}$-in -long plenum chamber, which was followed by a separately cooled converging-diverging nozzle section The supersonic flow (Mach number $\approx$ 2) from the nozzle was discharged into a water-cooled calorimeter and then exhausted to atmosphere Figure 1 is a diagram of the apparatus used Three separate nozzle sections were used having throat diameters of 0 125 0 137, and 0 210 in Two cathode designs were used with the 0 210-in throat and are also shown in Fig 1

Cooling water temperatures in the calorimeter lines were measured with calibrated thermocouple probes immersed in the flow and were read on manually balanced precision potentiometers Water mass flow rates in the calorimeter were measured with a precision bore flowmeter calibrated after being installed in the calorimeter system Air mass flow rates were measured with a calibrated orifice using a differential pressure transducer and an oscillograph The temperature of the air exhausting from the calorimeter was measured with a total temperature probe and read on a Brown recorder Profiles of the exit air temperature were obtained for all reported data, and a check of total pressure across the calorimeter exit showed a variation of less than $\frac{1}{4}\%$ of centerline pressure between the centerline and outer wall Measured heat losses from the calorimeter to room air amounted to 1% of the total heat flux through the calorimeter, and a correction was made in the data reduction for these losses Heat losses to the nozzle section were obtained by measuring water flow rates through the section with turbine type flowmeters, and temperature changes were measured with thermocouples immersed in the cooling lines It is felt that the uncertainty of the entire calorimeter and air mass flow system was no more than $\pm 6\%$

Sonic Throat Technique

A currently useful means of obtaining stagnation chamber enthalpy levels is through use of a sonic throat analysis By the assumption of a one-dimensional, isentropic expansion from stagnation chamber to sonic throat conditions, the stagnation enthalpy can be related to the stagnation pressure, the mass flow, and the effective throat area A plot of this relationship for high-temperature air appears as chart 14 of Ref 2 In a similar fashion, a straight line fit to a plot of $\log (p_{t\,\text{hot}}\, A^*_{\text{hot}}/\dot{m}_{\text{hot}})$ vs $\log h^*$ can be used to give the following equation:

$$h^* = 0\ 00645 \left[\frac{p_{t,\,\text{hot}}\, A^*_{\text{hot}}}{\dot{m}_{\text{hot}}}\right]^{2\ 48} \text{Btu/lb} \qquad (1)$$

If it is assumed that $A^*_{h\,t} = A^*_{\text{geom}\,t\,i}$, measured values of stagnation pressure and the mass flow will then determine the sonic enthalpy in Eq (1) (h_t can easily be obtained from h^*) Cold, perfect gas (γ = 1 4) relations can be introduced in

the form of a quotient that is constant, and Eq (1) can be written as

$$h^* = 0\ 0312\ T_t^{1\ 24}{}_{c\ ld} \left[\frac{\dot{m}_{cold}\ p_{t,\ hot}}{p_{t\ c\ ld}\ \dot{m}_{h\ t}} \right]^{2\ 48} \text{Btu/lb} \qquad (2)$$

In Eq (2) it has been assumed that $(A^*_{h\ t}/A^*_{cold}) = 1$ A discussion of the development of these equations appears in the Appendix of Ref 3 In Ref 3 the exponent on $(p_t A^*/\dot{m})$ was written as 2 5; however, for the range of enthalpy considered here a slightly better fit (to computed data in Ref 2) is obtained with an exponent of 2 48

Results

A plot of h_t as determined by Eq (2) against h_t as determined by the calorimeter is shown in Fig 2 Figure 2 also shows a plot of h_t as determined from measured air mass flow, stagnation pressure, and the geometric throat area using the computed results of Ref 2 against h_t as determined by the calorimeter It is apparent that use of the method whereby the geometric throat area is substituted into Eq (1) (or into computed results) introduces large errors in the stagnation enthalpy determination As throat size increased to 0 210, this error decreased as would be expected The scatter in the data when h_t is obtained using the geometric throat area reflects another important point From an experimental standpoint the stagnation enthalpy is a function of $(d^*)^{4\ 96}$ in Eq (1), so that even small variations of the throat size can cause large variations in the determination of stagnation enthalpy Such variations are, of course, aggravated by the use of small throats

One effect of increasing the throat size was an increase in the ratio (power to air)/(total power input), but because of the higher air mass flow, little gain in the stagnation enthalpy was obtained With the largest throat used however, introduction of a newly designed cathode (cathode number 2 shown in Fig 1) resulted in a 50% increase in the stagnation enthalpy In analyzing the results with the two cathodes, the throat discharge coefficient was computed for each case The discharge coefficient is defined as the ratio

$$\frac{\dot{m}_{actual}}{\dot{m}_{id\ l}} = \frac{\rho^* A^*_{effective}\ u^*}{\rho^* A^*_{g\ m\ t\ i}\ u^*}$$

The calculations showed that the throat discharge coefficient under hot conditions remained the same for both cathodes Under cold conditions, however, the discharge coefficient was lower with cathode number 1, which indicates

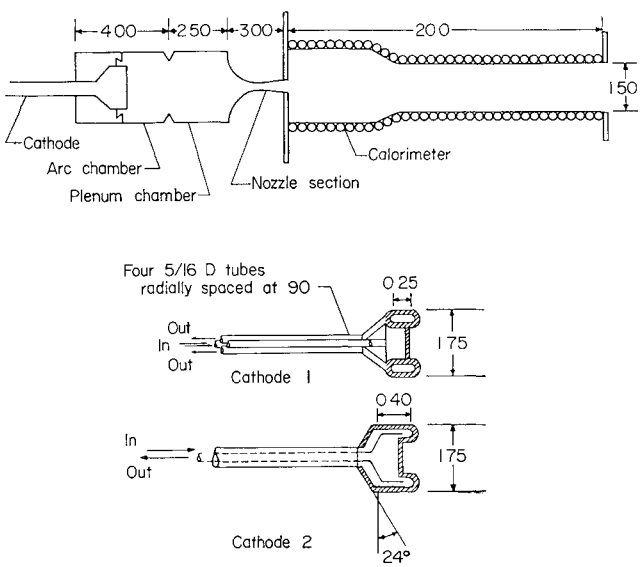

Fig 1 Arc-heater configurations with attached sonic nozzle and calorimeter

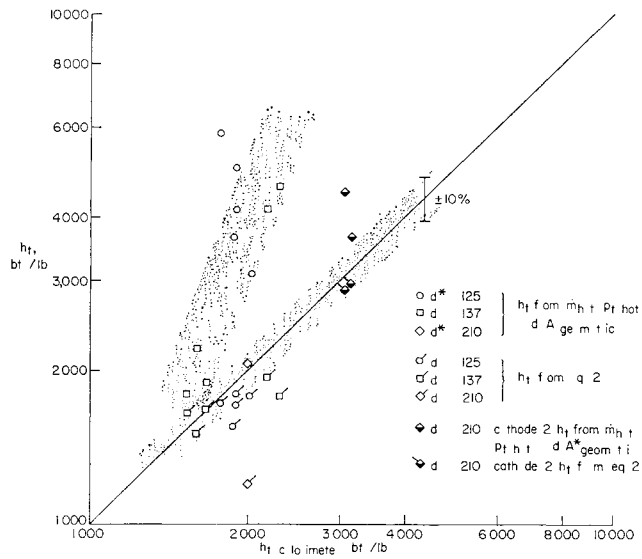

Fig 2 Total enthalpy determined using two sonic throat techniques vs calorimeter enthalpy

that swirl and a more turbulent flow exist with cathode number 1 A typical result using Eq (2), cathode number 1, and the 0 210 in throat is shown in Fig 2 Measurements of heat losses to the electrodes showed that cathode number 1 had losses 27% higher than cathode number 2 At the same time cathode number 1 losses were measured, the anode losses were measured as 75% above anode losses when cathode number 2 was used It is concluded from these measurements that the increased performance with cathode number 2 is, in fact, due primarily to a less turbulent gas flow in the region of the arc

It was desired to test the assumption that $A^*_{hot}/A^*_{cold} = 1$, and thus the usefulness of Eq (2) over a range of operating conditions The cold stagnation pressure was varied from 3 to 8 atm giving corresponding hot stagnation pressures from 10 to 22 atm, and the results are shown for Eq (2) in Fig 2 In this pressure range the mass flow for cold and hot runs was nearly the same, and the throat discharge coefficients did not vary between cold and hot conditions Correspondingly good agreement is seen in Fig 2 between the enthalpy as determined by the calorimeter and by the use of Eq (2) A number of runs were made with the cold stagnation pressure set at 11 atm, and the results (not shown) using the 0 137-in throat and Eq (2) gave a gross underestimation of the stagnation enthalpy The cause for the failure of Eq (2) to give agreement with the calorimeter results for these tests stems from the fact that air was injected into the arc chamber tangential to the outer walls, and as the mass flow was increased the effects of swirl increased in the nozzle The cold discharge coefficient at these high-mass flow rates dropped to a low value of about 0 55 because of the increased swirl Under the corresponding hot conditions for this series of runs the discharge coefficient was relatively high ($C_d \approx 0\ 90$)

These results indicate that Eq (2) can be used for enthalpy determination if care is taken to properly select the cold operating conditions so that the throat discharge coefficient remains constant between cold and hot operation of the heater

Conclusions

Although the results of this study are probably quite specific, being highly dependent on heater geometry, they do demonstrate that large errors in stagnation enthalpy determination are possible when it is assumed that the effective throat area during hot operation is equal to the geometric throat area In addition, if a sonic throat equation is to be used that employs the assumption that displacement effects

in the throat are the same between cold and hot operating conditions, it is evident that a close check must be made on the range of operating conditions that will give a valid determination of the stagnation enthalpy level in a particular facility

References

[1] Boatright, W B, Stewart, R B, and Grimaud, J E, "Description and preliminary calibration tests of a small arc-heated hypersonic wind tunnel," NASA TN D-1377 (December 1962)

[2] Jorgensen, L H and Baum, G M, "Charts for equilibrium flow properties of air in hypervelocity nozzles," NASA TN D 1333 (September 1962)

[3] Grimaud, J E and McRee, L C, "Exploratory investigation of heat transfer reduction and variation of shock stand off distance with fluid injection cooling on a hemisphere cone in an arc-heated hypersonic airstream," NASA Tech Memo (to be published)

Temperature Recovery Factors for Flow Longitudinal to a Circular Cylinder

E M Sparrow* and D P Fleming†
University of Minnesota, Minneapolis, Minn

THE axisymmetric flow longitudinal to the exterior of a circular cylinder differs from the flow along a flat plate due to the transverse curvature of the cylindrical surface The extent to which the velocity field about the cylinder deviates from that for the flat plate has been analyzed by Seban and Bond,[1] who also investigated the corresponding heat-transfer problem for a gas with a Prandtl number of 0 715 The Seban-Bond analysis yields expressions for skin friction, heat transfer, and recovery factor in the form of series; the first term of each series corresponds to the flat-plate problem, and succeeding terms give the deviations due to transverse curvature Quantitative results were obtained from numerical solutions of a set of ordinary differential equations of the boundary-layer type An improvement in the accuracy of the velocity solutions was later achieved by Kelly,[2] who made use of an analog computer in lieu of desk calculators employed by the original investigators Within the knowledge of the present authors, the thermal results reported by Seban and Bond still stand without re-examination

It is the purpose of this investigation to re-examine the recovery-factor result of Seban and Bond and also to provide recovery-factor information for a wide range of gas Prandtl numbers The need for results encompassing a more extensive Prandtl-number range is highlighted by such applications as the recovery-factor method[3] of measuring the Prandtl number In the forthcoming presentation, the nomenclature of the Seban-Bond paper will be employed whenever possible to facilitate a concise description

One may begin by relating the recovery factor R to the dimensionless boundary-layer temperature distribution $g(\xi,\eta) = (T - T_\infty)/(U_\infty^2/c_p)$ Under the adiabatic-wall condition, the surface temperature of the cylinder may be designated as T_{aw} and the recovery factor written as

$$R = (T_{aw} - T_\infty)/(U_\infty^2/2c_p) = 2g(\xi,0) \tag{1}$$

The temperature distribution g is expressible as a perturbation series

$$g(\xi,\eta) = g_0(\eta) + \xi g_1(\eta) + \xi^2 g_2(\eta) + \tag{2}$$

Received November 19, 1963

* Professor of Mechanical Engineering, Heat Transfer Laboratory

† Research Assistant, Heat Transfer Laboratory

Table 1 Wall derivatives of the velocity function f

	Seban-Bond	Kelly	Present
$f_1''(0)$	0 704	0 696	0 694322
$-f_2''(0)$	0 095	0.160	0.164144

wherein the coordinates ξ, η are defined in terms of the radial coordinate r, the axial coordinate x, the cylinder radius a, and other standard symbols as

$$\xi = (4/a)\ (\nu x/U_\infty)^{1/2}$$
$$\eta = (U_\infty/\nu x)^{1/2}[(r^2 - a^2)/4a] \tag{3}$$

It may be seen that η is a generalization of the Blasius simi larity variable which is defined as zero at the cylinder surface $r = a$, and ξ is a stretching of x which is proportional to the ratio of the boundary-layer thickness to the cylinder radius a The transverse curvature effect vanishes as $\xi \to 0$; correspondingly, $g_0(\eta)$ can be identified as the temperature distribution for the flat-plate problem

The temperature solution is carried out by substituting the g series into the energy equation along with a corresponding series for the dimensionless stream function f When terms are grouped according to powers of ξ, there emerges a set of ordinary differential equations for the functions g_0, g_1, g_2, etc The governing equations for g_0 and g_1 are available in Ref 1, Eqs (27) and (28) For g_2, one finds

$$(1/Pr)g_2'' + f_0 g_2' - 2f_0' g_2 + (1/Pr)(\eta g_1'' + g_1') + 2f_1 g_1' - f_1' g_1 + 3f_2 g_0' + \tfrac{1}{2} f_0''(f_2'' + \eta f_1'') + \tfrac{1}{4}(f_1'')^2 = 0 \tag{4}$$

where the primes denote differentiation with respect to η, and f_0, f_1, and f_2 are functions which appear in the series for f The boundary conditions appropriate to the adiabatic wall problem are $g_i'(0) = 0$ and $g_i(\infty) = 0$ for all i

To proceed, it is necessary that numerical solutions be performed These were carried out to high accuracy on a Con trol Data 1604 digital computer The differential equations involved in the problem are linear except for the f_0 (Blasius) equation Consequently, it was possible to construct solutions of each equation by linearly combining pairs of trial functions that satisfied the differential equation and the boundary conditions at $\eta = 0$

In order to obtain highly accurate temperature solutions, it was initially necessary to solve for the velocity functions f_0, f_1, and f_2 The quantities that essentially characterize these solutions are $f_0''(0)$, $f_1''(0)$, and $f_2''(0)$ These same quantities appear directly in the skin-friction expression The numerical value of $f_0''(0) = 1\ 32823$ is immediately recognizable as corresponding to the Blasius solution The values of $f_1''(0)$ and $f_2''(0)$ are listed in Table 1 to facilitate comparison with the prior investigations, Refs 1 and 2 It is seen from the table that the present velocity solutions represent an additional refinement relative to Kelly's recalculation of the Seban-Bond results

The quantities that are characteristic of the temperature solutions are $g_0(0)$, $g_1(0)$, $g_2(0)$, By applying Eqs (1) and (2), it follows that these same quantities appear in the recovery-factor expression

$$R/R_{fp} = 1 + \xi[g_1(0)/g_0(0)] + \xi^2[g_2(0)/g_0(0)] + \tag{5}$$

in which R_{fp}, the recovery factor for the flat plate, is given by

$$R_{fp} = 2g_0(0) \tag{5a}$$

The departures of R/R_{fp} from unity are a direct measure of the effect of transverse curvature on the recovery factor

Numerical values of the $g(0)$ quantities are listed in Table 2 for the Prandtl number range 0 6 to 1 1 Inspection of the table reveals several interesting trends First of all, it appears that the transverse curvature effect vanishes when the Prandtl number is unity, i e, $g_1(0) = g_2(0) = 0$ Corre-